Proc. Estonian Acad. Sci. Engng., 1998, 4, 2, 144–160
https://doi.org/10.3176/eng.1998.2.07

# NUMERICAL SIMULATION OF THE DISTRIBUTION CHARACTERISTICS OF FINE SOLID PARTICLES IN A HORIZONTAL PIPE

Alexander KARTUSHINSKY

Department of Aeromechanics, Estonian Energy Research Institute, Paldiski mnt. 1, EE-0001 Tallinn, Estonia; e-mail: aeromeh@online.ee

Received 21 February 1997, in revised form 30 December 1997

**Abstract.** Using a special model for the closure of the driving equations of the dispersed phase, the behaviour of fine solid particles in the two-phase turbulent flow in a horizontal pipe is investigated. The model is based on inter-particle collisions, since the dispersed phase is considered here as a polydispersed phase. The pseudo-viscosity coefficients are introduced in the driving equations of the dispersed phase, which allows for the description of an additional diffusive transfer of mass, momentum and angular momentum in the equations of the particles. Along with the inter-particle collisions, the Saffman and the Magnus lift forces are taken into account. All these factors together yield the distribution of mass concentration across the pipe, which is similar to our experimental observations.

**Key words:** inter-particle collision, pseudo-viscosity coefficients, distribution of mass concentration.

## 1. INTRODUCTION

In practice, we often encounter particulate two-phase turbulent flows, e.g., pneumatic conveying, cyclone separators, and transport of pulverized coal in power plants. The confinement may considerably influence the motion of the dispersed phase by inter-particle collisions, particle-wall collisions, and lift forces. Our experimental studies of the two-phase flows with solid particles have shown that the dispersed phase moves with the velocity lag (particles lag behind the gas) when conveying rough particles. However, the velocity lag disappears when fine particles are conveyed. At the same time, the particles in the horizontal pipe are distributed either with increasing mass concentration towards the pipe axis or with a growth in mass concentration towards the wall, depending

on their size [1,2]. Many experiments have described the two-phase turbulent vertical pipe [3,4] and channel flow [5] to eliminate the asymmetry in two-phase flows. Unfortunately, insufficient attention has been paid to the motion and distribution characteristics of fine particles discovered and described in [1,2].

This investigation focuses on the motion of fine particles in a horizontal pipe to describe the variety of the distribution of particle mass concentration across the pipe [1,2]. The goal is to develop a mathematical model describing the distribution characteristics of fine particles. The model is characterized by the implementation of inter-particle collisions for the closure of the driving equations of the dispersed phase.

The mathematical simulation of two-phase turbulent flows has been performed by the Lagrangian [6,7] or the Eulerian method [8,9]. The latter requires closure models for both phases. The authors of [8] closed the equations of the dispersed phase within the equilibrium approach, suggesting the transport equation for the kinetic energy of particles, using the theory of rapid granular flows [10], where the effect of inter-particle collisions dominates the turbulent diffusion of particles. On the other hand, using the inter-particle collisions, the authors of [9] suggested the driving equations for each component of the stress tensor of both phases (non-equilibrium approach for the closure). Unlike the differential closure models in [8,9], which require establishing the boundary conditions for each component of the stress tensor, our closure model is an algebraic closure model free from the problems above. This model suggests an introduction of the pseudo-viscosity coefficients in the transport equations of the dispersed phase. These pseudo-viscosity coefficients are obtained analytically, using the mechanism of the binary collision of particles. This model allows for the description of the distribution characteristics in a horizontal pipe.

## 2. MATHEMATICAL MODEL AND EQUATIONS

Mathematical modelling is carried out within the Eulerian method for the dispersed phase, while this phase itself is considered as a multi-velocity continuum [11]. The interaction of solid particles with the gaseous phase is described by the viscous drag force. In addition, the Magnus and the Saffman lift forces are taken into account. Other force factors are negligible since the ratio of particle density to the that of gas is large. We neglect the influence of the gravitational force since the settling velocity of fine particles is by a factor of $10–10^2$ lower than particle velocity, caused by inter-particle collisions or the Saffman force. For this reason, an axisymmetrical two-phase flow in a horizontal pipe is considered.

The internal friction in the dispersed phase is caused by inter-particle collisions. The real manufactured powders used in our experiments are polydispersed with up to 30% dispersion of the particle size.

The distribution of particle mass versus particle size for powders with the weighted mean particle size $\delta = 17$ and 32 μm are shown in Figs. 1 and 2, respectively. In order to simplify the description of the motion in the poly-dispersed phase, we introduce three particle fractions in the composition of the dispersed phase, i.e., we consider the transport of three particle fractions: the main particle fraction with large mass contribution (index 2) and two additional particle fractions with small mass contributions (indices 1 and 3). Such a dispersed phase is characterized by the following quantities: the particle size of the fractions $\delta_1 < \delta_2 < \delta_3$; the velocity components in the streamwise and transversal directions $u_{s1}$, $v_{s1}$, $u_{s2}$, $v_{s2}$, $u_{s3}$, $v_{s3}$, respectively; the angular particle velocities $\omega_{s1}$, $\omega_{s2}$, $\omega_{s3}$, and the particle mass concentration of three particle fractions $\alpha_1, \alpha_2, \alpha_3$. The particle diameters of additional particle fractions (1, 3) were found 90 and 110% of the particle diameter of the main fraction, respectively. Furthermore, 50% of the mass contribution was equally distributed between two additional particle fractions (1) and (3), while the remaining 50% of the mass contribution was related to the main particle fraction (2).

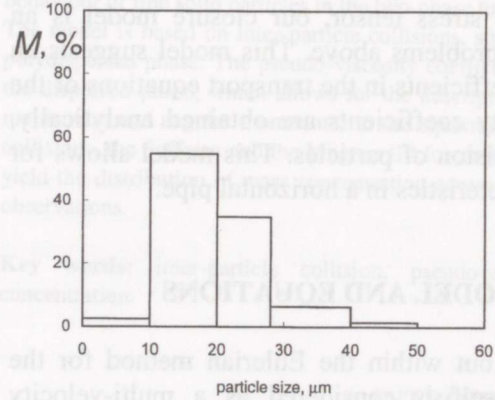


Fig. 1. Particle mass distribution for the particle size $\delta = 17$ μm.

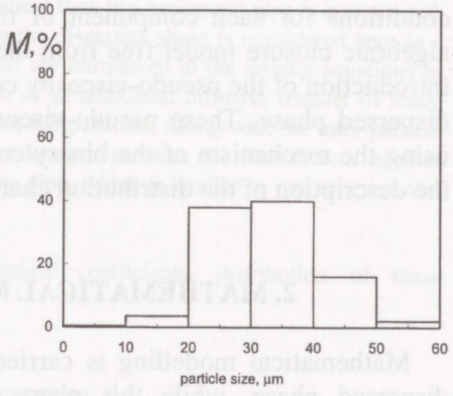


Fig. 2. Particle mass distribution for the particle size $\delta = 32$ μm.

The driving equations for the gaseous and dispersed phases were written, using the approximation of the turbulent boundary layer, where the turbulent transfer in the transverse direction is much stronger than in the direction of the main flow. For the closure of the driving equations in the gaseous phase, the $k-\varepsilon$ turbulence model is used, taking into account the influence of the wall. This influence is expressed in the introduction of the wall functions into the equations of the turbulent energy, and the rate of its dissipation is based on [12].

The driving equations for each particle fraction are expressed as

$$\frac{\partial(\alpha_i u_{si})}{\partial x}+\frac{1}{r}\frac{\partial(r\alpha_i v_{si})}{\partial r}=\frac{1}{r}\frac{\partial}{\partial r}rD_{si}\frac{\partial \alpha_i}{\partial r}, \quad (1)$$

$$u_{si}\frac{\partial u_{si}}{\partial x}+\left(v_{si}-\frac{\left(D_{si}+\nu_{si}^{1}\right)}{\alpha_i}\frac{\partial \alpha_i}{\partial r}\right)\frac{\partial u_{si}}{\partial r}$$
$$=\frac{1}{r}\frac{\partial}{\partial r}r\nu_{si}^{1}\frac{\partial u_{si}}{\partial r}+\frac{3\rho}{4\rho_p}\left[\frac{24C'_{Di}\nu(u-u_{si})}{\delta_i^2}-\Omega_i(v-v_{si})\right], \quad (2)$$

$$u_{si}\frac{\partial v_{si}}{\partial x}+\left(v_{si}-\frac{\left(D_{si}+\nu_{si}^{2}\right)}{\alpha_i}\frac{\partial \alpha_i}{\partial r}\right)\frac{\partial v_{si}}{\partial r}=\frac{1}{r}\frac{\partial}{\partial r}r\nu_{si}^{2}\frac{\partial v_{si}}{\partial r}$$
$$+\frac{3\rho}{4\rho_p}\left[\frac{24C'_{Di}\nu(v-v_{si})}{\delta_i^2}+(u-u_{si})\left(\Omega_i-\frac{4.1\cdot f_s\left(\mathrm{Re}_{pi},\mathrm{Re}_{\omega i}\right)}{\delta_i}\sqrt{\nu\frac{\partial u}{\partial r}}\right)\right], \quad (3)$$

$$u_{si}\frac{\partial \omega_{si}}{\partial x}+\left(v_{si}-\frac{\left(D_{si}+\nu_{si}^{3}\right)}{\alpha_i}\frac{\partial \alpha_i}{\partial r}\right)\frac{\partial \omega_{si}}{\partial r}=\frac{1}{r}\frac{\partial}{\partial r}r\nu_{si}^{3}\frac{\partial \omega_{si}}{\partial r}+60\frac{\rho\nu}{\rho_p}\frac{\Omega_i}{\delta_i^2}. \quad (4)$$

Here $\nu$ is the kinematic viscosity of gas; $\rho, \rho_p$ are the densities of gas and solid particle material, respectively; $\Omega_i=\frac{\partial u}{2\partial r}-\omega_{si}$ is the angular velocity slip; $C'_{Di}=1+0.278\cdot\sqrt{\mathrm{Re}_{pi}}+0.01388\cdot\mathrm{Re}_{pi}$ is the deviation of the drag coefficient from the Stokes friction [13], $\mathrm{Re}_{pi}=\sqrt{(u-u_{si})^2+(v-v_{si})^2}\,\delta_i/\nu$ is the Reynolds number of the particle. The function $f_s\left(\mathrm{Re}_{pi},\mathrm{Re}_{\omega i}\right)$ is determined from [14] as follows:

$$f_s\left(\mathrm{Re}_{pi},\mathrm{Re}_{\omega i}\right)=\left(1-0.23434\frac{\mathrm{Re}_{\omega i}}{\mathrm{Re}_{pi}}\right)\exp\left(-\frac{\mathrm{Re}_{pi}}{10}\right)+0.23434\frac{\mathrm{Re}_{\omega i}}{\mathrm{Re}_{pi}}\quad\left(\mathrm{Re}_{pi}\le 40\right), \quad (5)$$

$$f_s\left(\mathrm{Re}_{pi},\mathrm{Re}_{\omega i}\right)=0.0371\sqrt{\mathrm{Re}_{\omega i}}\quad\left(\mathrm{Re}_{pi}>40\right), \quad (6)$$

where the Reynolds number from the shear rate is $\mathrm{Re}_{\omega i}=\frac{\delta_i^2}{4\nu}\left|\frac{\partial u}{\partial r}\right|$.

This function characterizes the influence of the particle of Reynolds number $\mathrm{Re}_{pi}$ and the rotational Reynolds number $\mathrm{Re}_{\omega i}$ in the formulae for the Saffman force $D_{si}$, $\nu_{si}^{1}$, $\nu_{si}^{2}$, $\nu_{si}^{3}$ are the introduced pseudo-viscosity coefficients. The equations are those of the particle mass conservation (1), the momentum transfer

in the axial (2) and radial (3) directions, and the angular momentum transfer (4) of the particles.

We used the eddy-viscosity concept for the closure of the driving equations in the dispersed phase and introduced the pseudo-viscosity coefficients. The expressions for the second moments of the linear velocity components in the dispersed phase were taken from [9], and the Fick's law was used to obtain the expression for the correlation of the mass concentration and the particle velocity fluctuations. We also determined the second moment for the angular velocity of the particle in the gradient form like in [15]. Thus, we obtained the following expressions:

$$\left\langle u'_{si} v'_{si} \right\rangle = -\nu^1_{si} \frac{\partial u_{si}}{\partial r}, \tag{7}$$

$$\left\langle v'^2_{si} \right\rangle = -\nu^2_{si} \frac{\partial v_{si}}{\partial r} + \frac{2}{3} k_{si}, \tag{8}$$

$$\left\langle \omega'_{si} v'_{si} \right\rangle = -\nu^3_{si} \frac{\partial \omega_{si}}{\partial r}, \tag{9}$$

$$\left\langle \alpha'_i v'_{si} \right\rangle = -D_{si} \frac{\partial \alpha'_i}{\partial r}, \tag{10}$$

where $u'_{si}$, $v'_{si}$, $\omega'_{si}$, $\alpha'_i$ are the linear and angular fluctuating velocities of particles and the fluctuation of the mass concentration in the $i$-th particle fraction, respectively; $\nu^1_{si}, \nu^2_{si}, \nu^3_{si}$ and $k_{si}$ are the pseudo-viscosity coefficients and the coefficient of the kinetic energy exchange of the particles during collision.

The boundary conditions are written while particles slide along the wall ($w$):

$$u_{si}\big|_w = \gamma_u u_{si}\big|_w, \; v_{si}\big|_w = 0, \; \omega_{si}\big|_w = \gamma_\omega \omega_{si}\big|_w, \; \alpha_i v_{si}\big|_w = D_{si} \left.\frac{\partial \alpha_i}{\partial r}\right|_w, \tag{11}$$

where the coefficients $\gamma_u, \gamma_\omega$ characterize the losses of linear and angular momentum of particles. They are determined by the friction coefficient $k_t$ according to [16], since $\gamma_u = \dfrac{5+2k_t}{7}$ and $\gamma_\omega = \dfrac{2+5k_t}{7}$.

## 3. PSEUDO-VISCOSITY COEFFICIENTS

To define the pseudo-viscosity coefficients, let us assume that there are only binary particle collisions. Taking into account the restitution coefficients $k_{np}$ and $k_{tp}$ [16], the velocity differences of the linear and angular components before and after collision are

$$V_1' - V_1$$

$$= \beta_{21}\left\{(1-k_{np})[e\cdot(V_2-V_1)]\,e + \frac{(1-k_{tp})\,\xi}{(1+\xi)}\left[e\times(V_2-V_1) - \frac{(\delta_1\omega_1+\delta_2\omega_2)}{2}\right]\times e\right\}, \tag{12}$$

$$V_2' - V_2$$

$$= -\beta_{12}\left\{(1-k_{np})[e\cdot(V_2-V_1)]\,e + \frac{(1-k_{tp})\,\xi}{(1+\xi)}\left[e\times(V_2-V_1) - \frac{(\delta_1\omega_1+\delta_2\omega_2)}{2}\right]\times e\right\}, \tag{13}$$

$$\omega_1' - \omega_1 = \frac{\beta_{21}(k_{tp}-1)}{(1+\xi)}\left\{\frac{2}{\delta_1}e\times(V_2-V_1) + \omega_1 + \frac{\delta_2}{\delta_1}\omega_2 - \left(e\cdot\omega_1 + \frac{\delta_2}{\delta_1}e\cdot\omega_2\right)e\right\}, \tag{14}$$

$$\omega_2' - \omega_2 = \frac{\beta_{12}(k_{tp}-1)}{(1+\xi)}\left\{\frac{2}{\delta_2}e\times(V_2-V_1) + \omega_2 + \frac{\delta_1}{\delta_2}\omega_1 - \left(e\cdot\omega_2 + \frac{\delta_1}{\delta_2}e\cdot\omega_1\right)e\right\}, \tag{15}$$

where $e$ is the unity vector determined by the two angles $\varphi$, $\theta$ and the space parameter $\chi$ like in [16]; $V_1$, $V_2$ are the vectors of total velocity of particles 1 and 2 before their collision, respectively, their absolute values are determined as $V_1 = \sqrt{u_{s1}^2 + v_{s1}^2}$ and $V_2 = \sqrt{u_{s2}^2 + v_{s2}^2}$; $\omega_1$, $\omega_2$ are the vectors of angular velocity of particles 1 and 2 before their collision; the prime characterizes these values after collision.

The variables $\beta_{21}$ and $\beta_{12}$ are defined as $\beta_{21} = m_2/(m_1+m_2)$ and $\beta_{12} = m_1/(m_1+m_2)$, where $m_1$, $m_2$ are the masses of colliding particles. The parameter equal to 0.4 for a spherical particle is $\xi = 4\cdot I_i/m_i\delta_i^2$, where $I_i$ is the particle's rotary inertia. A schematic picture of the particle collision in a space and in a plane is shown in Figs. 3 and 4, respectively.

The velocity differences (Eqs. (12)–(15)) are considered here as the fluctuating velocities of a particle. To obtain the stress tensor components, let us multiply the different components of the fluctuating velocities and average the product over the two angles $\varphi$, $\theta$ and the space parameter $\chi$. We have then $\langle(u_{s21}' - u_{s2})(v_{s21}' - v_{s2})\rangle$, $\langle(v_{s21}' - v_{s2})^2\rangle$, $\langle(\omega_{s21}' - \omega_{s2})(v_{s21}' - v_{s2})\rangle$, $\langle(u_{s21}' - u_{s2})^2\rangle + \langle(v_{s21}' - v_{s2})^2\rangle$, etc. The averaging procedure is expressed as

$$\left\langle \left(u'_{sij}-u_{si}\right)\left(v'_{sij}-v_{si}\right)\right\rangle\Big|_{\theta,\chi,\varphi}$$

$$=\frac{1}{2\pi}\frac{1}{\varphi_{ij}}\frac{\int_0^{2\pi}d\theta\int_0^1\chi d\chi\int_0^{\varphi_{ij}}\left(u'_{sij}-u_{si}\right)\left(v'_{sij}-v_{si}\right)d\varphi}{\int_0^1\chi d\chi}. \tag{16}$$

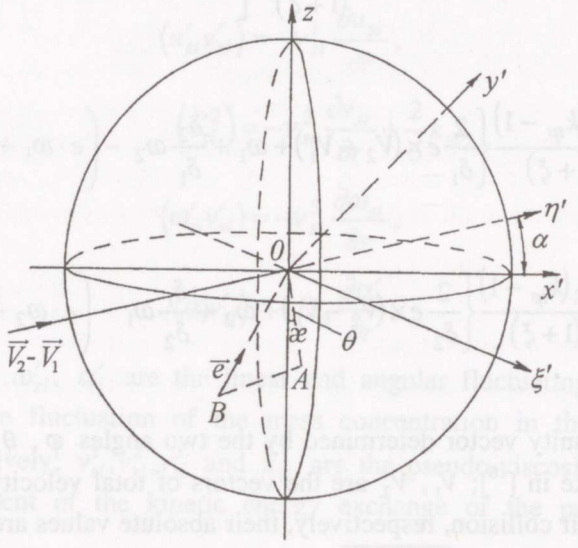


Fig. 3. Schematic diagram of the particle collision (in space).

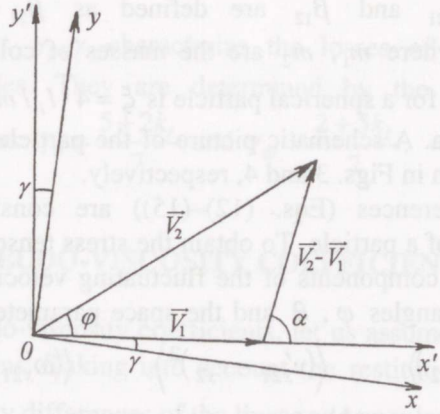


Fig. 4. Schematic diagram of the particle collision (in plane).

The averaging shows that the stress tensor components depend strongly on the angle $\varphi_{ij}$, determined as

$$\varphi_{ij} = \left| \operatorname{arctg} \left( \frac{v_{si}}{u_{si}} - \frac{v_{sj}}{u_{sj}} \right) \Bigg/ \left( 1 + \frac{v_{si} v_{sj}}{u_{si} u_{sj}} \right) \right|.$$

The pseudo-viscosity coefficients result from multiplying the stress tensor components by the time of inter-particle collisions $\Delta t$, which is determined through the probability of particle collisions, like in [17]. The probability of collision is determined in the simplest case of the binary collision of particles according to [18] as

$$P_{ij} = \frac{\pi}{4} \frac{\left(\delta_i + \delta_j\right)^2}{l_i^2}, \tag{17}$$

where $l_i$ is the inter-particle distance for the $i$-th particle fraction, determined by the particle mass concentration $\alpha_i$ as $l_i = \delta_i \sqrt[3]{\pi\rho/(6\rho_p \alpha_i)}$. The time of inter-particle collisions $\Delta t$ is determined by equalizing the probability of collision (17) to the probability of collision obtained in [17] as follows:

$$\Delta t = \frac{4 \cdot P_{ij}}{\pi \cdot \left(\delta_i + \delta_j\right)^2 n_j \left| V_j - V_i \right|}, \tag{18}$$

where $n_j$ is the volumetric numerical concentration of the $j$-th particle fraction and $\left| V_j - V_i \right|$ is the velocity difference at the time of the particle collision.

Dropping the manipulations and using the formulae

$$v_{si}^1 = \left\langle \left(u'_{sij} - u_{si}\right)\left(v'_{sij} - v_{si}\right) \right\rangle \Delta t;$$

$$v_{si}^2 = \left\langle \left(v'_{sij} - v_{si}\right)^2 \right\rangle \Delta t;$$

$$v_{si}^3 = \left\langle \left(\omega'_{sij} - \omega_{si}\right)\left(v'_{sij} - v_{si}\right) \right\rangle \Delta t;$$

$$D_{si} = \left[ \left\langle \left(u'_{sij} - u_{si}\right)^2 \right\rangle + \left\langle \left(v'_{sij} - v_{si}\right)^2 \right\rangle \right] \Delta t,$$

the pseudo-viscosity coefficients for three particle fractions are

$$v_{si}^k = g_0 \sum_{j=1, j \neq i}^{3} \frac{\beta_{ji}^2}{\sqrt[3]{\alpha_j}} \left(V_i + V_j\right) \delta_j X_{ij}^k. \tag{19}$$

To obtain the coefficient $k_{si}$, we multiply the square of the fluctuating velocity difference $\left\langle \left(u'_{sij} - u_{si}\right)^2 \right\rangle + \left\langle \left(v'_{sij} - v_{si}\right)^2 \right\rangle \Big|_{\theta,\chi,\varphi}$ to the probability of the particle collision (17) as follows:

$$k_{si} = \sum_{j=1,\, j\neq i}^{3} \beta_{ji}^2 \left(V_i + V_j\right)^2 P_{ij} Y_{ij}, \tag{20}$$

where the indices are $i, j = 1,2,3$; $k = 1,2,3,4$ and $g_0 = \sqrt[3]{\dfrac{\pi\rho_p}{6\rho}}$; the coefficients $X_{ij}^k$ and $Y_{ij}$ are defined in the Appendix.

The pseudo-viscosity coefficients (19) and the coefficient $k_{si}$ are entered on the right-hand side of the driving equations in the diffusive terms (Eqs. (1)–(4)) and the formulae ((7)–(10)). Here the properties of the flow are taken into account by the help of the linear and angular particle velocities, mass concentration, the relaxation parameters of the particles, including the particle material density and particle size and the collision coefficients, including the two restitution coefficients.

## 4. RESULTS AND DISCUSSION

The numerical calculations were conducted for a horizontal pipe and compared with the experimental data of [1,2] in the cross-section $200D$ downstream (here $D$ is the pipe diameter) at the outlet of the flow. The distribution of the gas velocity and the velocity of the dispersed phase determined as $U_s = \left(\alpha_1 u_{s1} + \alpha_2 u_{s2} + \alpha_3 u_{s3}\right)/\left(\alpha_1 + \alpha_2 + \alpha_3\right)$ are presented in the dimensionless form, like $U_s(r)/U(0)$ in various cross-sections ($X = 0$; $25D$; $200D$) in Figs. 5 and 6. Here $U(0)$ is the gas velocity at the axis of the pipe. The electrocorundum particles with the material density $\rho_p = 3950$ kg/m$^3$ and with sizes $\delta = 7$, 17 and 32 μm and with mass loading of 0.34 kg dust/kg air are used in a stainless steel pipe ($D = 35$ mm), and the particles with the size $\delta = 23$ μm and with mass loading of 0.62 kg dust/kg air are used in a smaller pipe ($D = 16$ mm). The outflow velocity (velocity over the cross-section of the pipe) was 50 m/s in both cases, then the Reynolds numbers are $\mathrm{Re} = u \cdot D/\nu = 116\,760$ and 53 300, respectively. The distribution of the mass concentration of the dispersed phase determined as $\alpha = \alpha_1 + \alpha_2 + \alpha_3$ is presented in the dimensionless form like $\alpha(r)/\alpha(0)$ in various cross-sections in Figs. 7 and 8. Here $\alpha(0)$ is the particle mass concentration at the axis of the pipe.

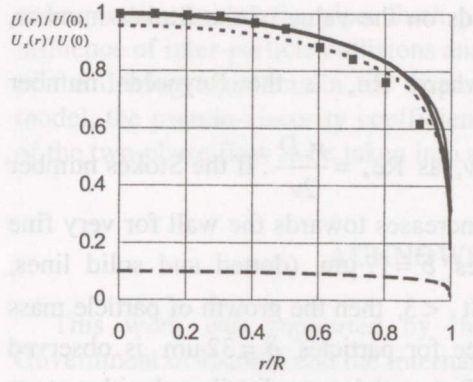


Fig. 5. Velocity of gas and particles in various cross-sections: — gas; particles: - - - $X = 0$, - - - $X = 25D$, ___ $X = 200D$; ■ exp. ($\delta = 32$ μm, $D = 35$ mm).

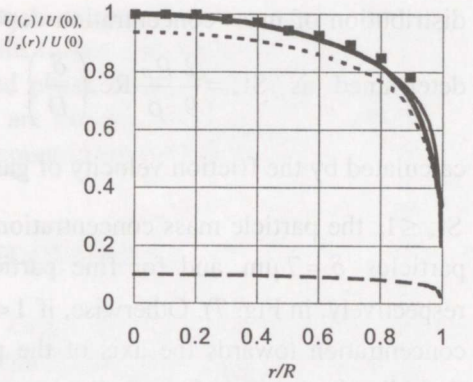


Fig. 6. Velocity of gas and particles in various cross-sections: — gas at $X = 200D$; particles: - - - $X = 0$, - - - $X = 25D$, ___ $X = 200D$; ■ exp. ($\delta = 25$ μm, $D = 16$ mm).

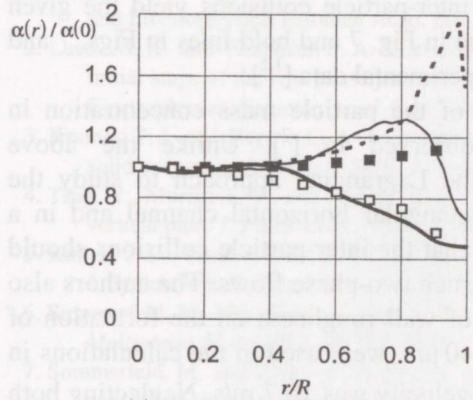


Fig. 7. The particle mass distribution for particles of different sizes at $X = 200D$, $D = 35$ mm: - - - $\delta = 7$ μm; $\delta = 17$ μm: — calc., ■ exp. $\delta = 32$ μm: ___ calc., □ exp.

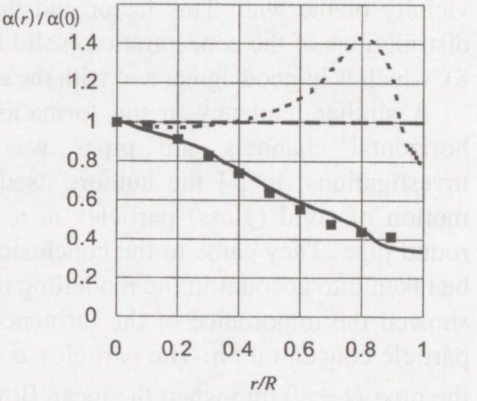


Fig. 8. The particle mass distribution in various cross-sections: — gas at $X = 200D$; particles: - - - $X = 0$; - - - $X = 25D$; ___ $X = 200D$; ■ exp. ($\delta = 25$ μm; $D = 16$ mm).

We started our calculations when initial particle velocity was 10% of the gas velocity (dashed lines in Figs. 5 and 6) in order to trace the development of the particle velocity and mass concentration along the whole pipe length, including its non-steady sections. From the non-steady sections, where the particles speed up to the region of the fully developed steady flow, the distribution of mass concentration transforms from the uniform distribution at the inlet to the non-uniform distribution with the growth in mass concentration towards the axis of the pipe at the outlet, passing the intermediate distribution with a wave-like profile (dotted line in Fig. 8). The analysis of the flow parameters shows that the

distribution of mass concentration depends on the value of the Stokes number, determined as $\mathrm{St}_* = \frac{2}{9}\frac{\rho_p}{\rho}\mathrm{Re}_*\left(\frac{\delta}{D}\right)^2$, where $\mathrm{Re}_*$ is the Reynolds number calculated by the friction velocity of gas $v_*$ as $\mathrm{Re}_* = \frac{v_* D}{2\nu}$. If the Stokes number $\mathrm{St}_* \le 1$, the particle mass concentration increases towards the wall for very fine particles $\delta = 7\,\mu\mathrm{m}$ and for fine particles $\delta = 17\,\mu\mathrm{m}$ (dotted and solid lines, respectively, in Fig. 7). Otherwise, if $1 < \mathrm{St}_* < 3$, then the growth of particle mass concentration towards the axis of the pipe for particles $\delta = 32\,\mu\mathrm{m}$ is observed (bold line in the same figure). As shown, fine particles are distributed with a steep growth in the mass concentration towards the wall. If $1 < \mathrm{St}_* < 3$, a non-uniform distribution of mass concentration of the particles $\delta = 23\,\mu\mathrm{m}$ with the growth towards the axis of the pipe can be seen for a narrow pipe $D$ = 16 mm (bold line in Fig. 8). Our numerical calculations show that the Saffman force is significant in the vicinity of the wall. This factor and the inter-particle collisions yield the given distributions of the concentration (solid line in Fig. 7 and bold lines in Figs. 7 and 8), which is in good agreement with the experimental data [1,2].

A similar tendency in the formation of the particle mass concentration in horizontal channels and pipes was observed in [7]. Unlike the above investigations, in [7] the authors used the Lagrangian approach to study the motion of solid (glass) particles in a rectangular horizontal channel and in a round pipe. They came to the conclusion that the inter-particle collisions should be taken into account in the modelling of such two-phase flows. The authors also showed the importance of the influence of wall roughness on the formation of particle concentration. The particles $\delta = 40\,\mu\mathrm{m}$ were used in the calculations in the pipe $D$ = 80 mm when the mean flow velocity was 10.7 m/s. Neglecting both the inter-particle collisions and wall roughness in the numerical simulation of the motion of glass particles in a smooth glass pipe resulted in particle accumulation at the bottom of the wall due to gravity [7]. Otherwise, if the above factors were taken into account, the distribution of mass concentration in stainless steel, considered as a rough pipe, would be axisymmetrical with the maximum concentration at the axis of the pipe [7]. This is in agreement with our results. The Reynolds number was 57 000 in [7], close to our flow conditions.

## 5. CONCLUSIONS

The given mathematical model describes a non-slip velocity motion of the dispersed phase with fine solid particles accompanied by a variety of profiles of particle mass concentration in a horizontal pipe. The Stokes number is a criterial parameter which allows one to describe the distribution characteristics of mass

concentration across the pipe. Such particle motion results from the combined influence of inter-particle collisions and lift forces. The elaborated closure model of the driving equations in the dispersed phase is an algebraic model. In this model, the pseudo-viscosity coefficients are introduced, allowing the properties of the two-phase flow to be taken into account in the calculations.

## ACKNOWLEDGEMENT

This work was supported by the Grant of the Joint Program of the Government of Estonia and the International Science Foundation No LK 6100.

## REFERENCES

1. Navoznov, S. I., Paveljev, A. A., Mulgi, A. S., and Laats, M. K. Effect of initial slip on admixture dispersion in two-phase jet. In *Turbulent Two-phase Flows.* Inst. Thermophysics and Electrophysics, Estonian Acad. Sci., Tallinn, 1979, 119–157 (in Russian).
2. Laats, M. K. and Frishman, F. A. The motion and dispersion of fine solid admixture in the initial stage of the two-phase jet. In *Turbulent Two-phase Flows.* Inst. Thermophysics and Electrophysics, Estonian Acad. Sci., Tallinn, 1979, 158–166 (in Russian).
3. Kramer, T. J. and Depew, C. A. Experimentally determined mean flow characteristics of gas-solid suspensions. *Trans. ASME, J. Basic Engineering,* 1972, Ser. D, 2, 254–262.
4. Tsuji, Y., Morikava, Y., and Shiomi, H. LDV measurements of an air-solid two-phase flow in a vertical pipe. *J. Fluid Mech.*, 1984, **139**, 417–434.
5. Kulick, J. D., Fessler, J. R., and Eaton, J. K. Particle response and turbulence modification in fully developed channel flow. *J. Fluid Mech.*, 1994, **277**, 109–134.
6. Sommerfeld, M. Modelling of particle-wall collisions in confined gas-particle flows. *Int. J. Multiphase Flow*, 1992, **18**, 905–926.
7. Sommerfeld, M. and Zivkovic, G. Recent advances in the numerical simulation of pneumatic conveying through pipe systems. In *Computational Methods in Applied Science* (Hirsch, Ch., ed.). Elsevier, B.V., 1992, 201–212.
8. Louge, M. Y., Mastorakos, E., and Jenkins, J. T. The role of particle collisions in pneumatic transport. *J. Fluid Mech.*, 1991, **231**, 345–359.
9. He, J. and Simonin, O. Non-equilibrium prediction of the particle-phase stress tensor in vertical pneumatic conveying. *Proc. 5th Int. Symp. on Gas-Solid Flows.* ASME FED, 1993, **166**, 253–263.
10. Jenkins, J. T. and Savage, S. B. A theory for the rapid flow of identical, smooth, nearly elastic, spherical particles. *J. Fluid Mech.*, 1983, **130**, 187–202.
11. Nigmatulin, R. I. *Fundamentals of Mechanics of Heterogeneous Media,* 1. Nauka, Moscow, 1978 (in Russian).
12. Durst, F. and Rastogi, A. K. Calculations of turbulent boundary layer flows with drag reducing polymer additives. *Phys. Fluids*, 1977, **20**, 1975–1985.
13. Kravtsov, M. V. Drag to the free steady motion of a sphere in viscous medium. *J. Engng. Phys.*, 1968, **XV**, 464–470 (in Russian).
14. Mei, R. An approximate expression for the shear lift force on a spherical particle at finite Reynolds number. *Int. J. Multiphase Flow*, 1992, **18**, 145–147.
15. Tennekes, H. and Lumley, J. L. *A First Course in Turbulence.* MIT, Boston, 1972.

16. Babukha, G. L. and Shraiber, A. A. *Introduction of Particles of Polydispersive Material in Two-phase Flows.* Naukova Dumka, Kiev, 1972 (in Russian).
17. Marble, F. E. Mechanism of particle collision in one-dimensional dynamics of gas-particle admixture. *Phys. Fluids*, 1964, **7**, 1270–1282.
18. Trushin, G. I. and Lipatov, N. N. The probability of collision of the suspended particles at their oriented motion. *Izv. Vysshikh Uchebnykh Zavedenii. Pishchevaya Tekhnol.*, 1963, 5, 110–114 ( in Russian).

## APPENDIX

## COEFFICIENTS $X_{ij}$ AND $Y_{ij}$

$$X_{ij}^1 = \left\{ g_1 \left[ (A_{ij} - C_{ij}) \sin 2\gamma_i - B_{ij} \cos 2\gamma_i \right] + g_2 R_{ij} \left( D_{ij} \cos 2\gamma_i - F_{ij} \sin 2\gamma_i \right) \right.$$
$$\left. + g_3 R_{ij}^2 \left[ \sin 2\gamma_i \left( G_{ij} - \frac{Q_{ij}}{2} \right) + H_{ij} \cos 2\gamma_i \right] \right\}, \tag{A1}$$

$$X_{ij}^2 = \left\{ g_4 A_{ij} + g_1 \left( 2A_{ij} \sin^2 \gamma_i - B_{ij} \sin 2\gamma_i - C_{ij} \cos 2\gamma_i \right) \right.$$
$$+ g_2 R_{ij} (D_{ij} \sin 2\gamma_i + F_{ij} \cos 2\gamma_i)$$
$$\left. + g_3 R_{ij}^2 \left[ Q_{ij} (1 + \cos^2 \gamma_i) - G_{ij} \cos 2\gamma_i + H_{ij} \sin 2\gamma_i \right] \right\}, \tag{A2}$$

$$X_{ij}^3 = \left\{ g_5 (L_{ij} + M_{ij} \operatorname{tg} \gamma_i) + g_6 R_{ij} (N_{ij} \operatorname{tg} \gamma_i - O_{ij}) + g_7 R_{ij}^2 (P_{ij} - T_{ij} \operatorname{tg} \gamma_i) \right\}, \tag{A3}$$

$$X_{ij}^4 = g_8 A_{ij} + g_9 R_{ij}^2 Q_{ij}, \tag{A4}$$

$$Y_{ij} = g_8 \frac{A_{ij}}{Q_{ij}} + g_9 R_{ij}^2. \tag{A5}$$

Here $X_{ij}^k = X_{ji}^k$ $(i = 1, 3;\ j = 1, 3;\ i \neq j)$ and the pseudo-viscosity diffusion coefficient $D_{si} = \nu_{si}^4$. The coefficients $g_i$ are determined as

$$g_1 = \frac{1}{2} \left( \frac{a+b}{2} \right)^2, \quad g_2 = \frac{(2a+3b)b}{15}, \quad g_3 = \frac{b^2}{16}, \quad g_4 = \frac{1}{3} \left( \frac{a-b}{2} \right)^2, \quad g_5 = 2b(a-b),$$
$$g_6 = \frac{5}{4} b(5a+7b), \quad g_7 = b^2, \quad g_8 = \frac{1}{3} \left[ \left( \frac{a+b}{2} \right)^2 + a^2 + b^2 \right], \quad g_9 = \frac{3b^2}{16},$$

and other coefficients are

$$A_{ij} = \frac{\varphi_{ij}}{E^{ij}}\left(1 - \frac{k_{ij}^2}{2}\left(1 + \frac{\sin\varphi_{ij}}{\varphi_{ij}}\right)\right), \tag{A6}$$

$$B_{ij} = \frac{k_{ij}^2 \sin^2\frac{\varphi_{ij}}{2}}{E^{ij}}\left(1 - \frac{V_j}{V_i}\cos^2\frac{\varphi_{ij}}{2}\right), \tag{A7}$$

$$C_{ij} = \frac{k_{ij}^2}{4}\frac{V_j}{V_i}\frac{\varphi_{ij}}{E^{ij}}\left(1 - \frac{\sin 2\varphi_{ij}}{2\varphi_{ij}}\right), \tag{A8}$$

$$D_{ij} = 1 - \frac{2V_j\left(2 - k_{ij}^2\right)}{3V_i k_{ij}^2} + \frac{4V_j\left(1 - k_{ij}^2\right)K^{ij}}{3V_i k_{ij}^2 E^{ij}} - \frac{2V_j \sin\varphi_{ij}}{3V_i E^{ij}}\sqrt{1 - k_{ij}^2\cos^2\frac{\varphi_{ij}}{2}}, \tag{A9}$$

$$F_{ij} = \frac{\left(1 + \frac{V_j}{V_i}\right)\sqrt{1 - k_{ij}^2}}{E^{ij}}\left(1 - \sqrt{\frac{1 - k_{ij}^2\cos^2\frac{\varphi_{ij}}{2}}{1 - k_{ij}^2}}\right)$$

$$\times\left(1 - \frac{V_j}{V_i} + \left(1 + \frac{V_j}{V_i}\right)\frac{\sqrt{1 - k_{ij}^2}}{3}\left(1 + \sqrt{\frac{1 - k_{ij}^2\cos^2\frac{\varphi_{ij}}{2}}{1 - k_{ij}^2}} + \frac{1 - k_{ij}^2\cos^2\frac{\varphi_{ij}}{2}}{1 - k_{ij}^2}\right)\right), \tag{A10}$$

$$G_{ij} = \frac{V_j\varphi_{ij}}{V_i E^{ij}}\left(\frac{1 - k_{ij}^2}{k_{ij}^2} + \frac{1}{2}\left(1 + \frac{\sin\varphi_{ij}}{\varphi_{ij}}\right) - \frac{2\sqrt{1 - k_{ij}^2}}{\varphi_{ij}k_{ij}^2}\operatorname{arctg}\left(\frac{\operatorname{tg}\frac{\varphi_{ij}}{2}}{\sqrt{1 - k_{ij}^2}}\right)\right), \tag{A11}$$

$$H_{ij} = \left(\frac{V_j}{V_i}\sin^2\frac{\varphi_{ij}}{2} + \frac{1}{4}\left(1 - \frac{V_j^2}{V_i^2}\right)\ln\left(\frac{1 - k_{ij}^2\cos^2\frac{\varphi_{ij}}{2}}{1 - k_{ij}^2}\right)\right)\frac{1}{E^{ij}}, \tag{A12}$$

$$L_{ij} = \frac{k_{ij}}{3}\sqrt{\frac{V_j}{V_i}}\left(\frac{\sin\varphi_{ij}}{E^{ij}}\sqrt{1 - k_{ij}^2\cos^2\frac{\varphi_{ij}}{2}} + \frac{\left(1 - k_{ij}^2\right)K^{ij}}{k_{ij}^2 E^{ij}}\right) - \left(1 + \frac{\left(1 - 2k_{ij}^2\right)}{3k_{ij}}\sqrt{\frac{V_j}{V_i}}\right), \tag{A13}$$

$$M_{ij} = \frac{\left(1+\frac{V_j}{V_i}\right)}{3E^{ij}}\sqrt{1-k_{ij}^2}\left(1-\sqrt{\frac{1-k_{ij}^2\cos^2\frac{\varphi_{ij}}{2}}{1-k_{ij}^2}}\right), \tag{A14}$$

$$N_{ij} = \frac{\varphi_{ij}}{E^{ij}}\frac{\left(1-\frac{V_j\sin\varphi_{ij}}{V_i\varphi_{ij}}\right)}{\left(1+\frac{V_j}{V_i}\right)}, \tag{A15}$$

$$O_{ij} = \frac{V_j\sin^2\frac{\varphi_{ij}}{2}}{V_iE^{ij}}, \tag{A16}$$

$$P_{ij} = \left(1-\frac{V_j}{V_i}\right)\frac{K^{ij}}{E^{ij}}+1+\frac{V_j}{V_i}, \tag{A17}$$

$$R_{ij} = \left(\frac{\delta_i\omega_i+\delta_j\omega_j}{V_i+V_j}\right), \tag{A18}$$

$$T_{ij} = \frac{2\sqrt{1-k_{ij}^2}}{E^{ij}}\left(1+\frac{V_j}{V_i}\right)\left(1-\sqrt{\frac{1-k_{ij}^2\cos^2\frac{\varphi_{ij}}{2}}{1-k_{ij}^2}}\right), \tag{A19}$$

$$Q_{ij} = \frac{\varphi_{ij}}{E^{ij}}. \tag{A20}$$

The total velocity, incomplete elliptic integrals of the first and the second type and the modulus of integrals are

$$V_i = \sqrt{u_{si}^2+v_{si}^2}, \quad K^{ij} = \int_0^{\varphi_{ij}}\frac{d\varphi}{\sqrt{1-k_{ij}^2\cos^2\frac{\varphi}{2}}}, \quad E^{ij} = \int_0^{\varphi_{ij}}\sqrt{1-k_{ij}^2\cos^2\frac{\varphi}{2}}d\varphi,$$

$$k_{ij}^2 = \frac{4V_iV_j}{(V_i+V_j)^2},$$

respectively. In an asymptotic approximation for small angles $\varphi << 1$, the expressions for the coefficients $A_{ij}$, $B_{ij}$, $C_{ij}$, $D_{ij}$, $F_{ij}$, $G_{ij}$, $H_{ij}$, $L_{ij}$, $M_{ij}$, $N_{ij}$, $O_{ij}$, $P_{ij}$, $T_{ij}$, $Q_{ij}$ are transformed as

$$A_{ij} = \pm \frac{\left(1 - \frac{V_j}{V_i}\right)}{\left(1 + \frac{V_j}{V_i}\right)}, \tag{A21}$$

$$B_{ij} = \pm \frac{k_{ij}^2}{2} \varphi_{ij} \left(1 + \frac{V_j}{V_i}\right), \tag{A22}$$

$$C_{ij} = 0, \tag{A23}$$

$$D_{ij} = 1, \tag{A24}$$

$$F_{ij} = -\frac{2\varphi_{ij}}{\left(1 - \frac{V_j}{V_i}\right)} \frac{V_j}{V_i}, \tag{A25}$$

$$G_{ij} = 0, \tag{A26}$$

$$H_{ij} = \pm \frac{\varphi_{ij}}{\left(1 - \frac{V_j}{V_i}\right)^2} \frac{V_j}{V_i}, \tag{A27}$$

$$L_{ij} = k_{ij} \sqrt{\frac{V_j}{V_i} - 1}, \tag{A28}$$

$$M_{ij} = -\left(1 + \frac{V_j}{V_i}\right) \frac{k_{ij}^2 \varphi_{ij}}{4}, \tag{A29}$$

$$N_{ij} = \pm \frac{1}{2}, \tag{A30}$$

$$O_{ij} = \pm \varphi_{ij} \frac{V_j}{2V_i} \frac{\left(1 + \frac{V_j}{V_i}\right)}{\left(1 - \frac{V_j}{V_i}\right)}, \tag{A31}$$

$$P_{ij} = 2\frac{\left(1+\frac{V_j}{V_i}\right)}{\left(1-\frac{V_j}{V_i}\right)}, \tag{A32}$$

$$T_{ij} = -2\varphi_{ij}\frac{V_j}{V_i}\frac{\left(1+\frac{V_j}{V_i}\right)}{\left(1-\frac{V_j}{V_i}\right)^2}, \tag{A33}$$

$$Q_{ij} = \frac{1}{A_{ij}}. \tag{A34}$$

## MATEMAATILINE MUDEL PEENFRAKTSIOONILISE TAHKEFAASI LEVIKU KIRJELDAMISEKS TURBULENTSEL VOOLAMISEL HORISONTAALSES ÜMARTORUS

Aleksander KARTUŠINSKI

Kasutades tahkefaasi ülekandevõrrandite sulgemiseks spetsiaalselt väljatöötatud teoreetilist mudelit, mis põhineb tahkete osakeste faasisiseste põrkeprotsesside arvestamisel, on väikeste osakeste ($\delta/D < 10^{-3}$) puhul arvmodelleeritud kahefaasilist (gaas–tahked osakesed) voolust horisontaalses ümartorus. Edasikandevõrrandite sulgemisel on vaadeldud tahkefaasi polüdisperssena ning võrranditesse on sisse viidud tahkefaasi pseudoviskoossuse koefitsiendid. Osakeste põrkeprotsesside ja tõusujõudude arvestamine võimaldab täpsemalt määrata erineva suurusega osakeste jaotust kanali ristlõikes. Arvmodelleerimise tulemused on rahuldavas kooskõlas eksperimendist saadud tahkefaasi kiirus- ja kontsentratsioonijaotusega.